Control of Quadrupedal Bounding with Flexible Torso and Speed Transitions with Sums of Squares Verification

Qu Cao[1], Evangelos Papadopoulos[2] and Ioannis Poulakakis[1†]

[1]Department of Mechanical Engineering, University of Delaware, Newark, DE, USA
(E-mail: caoqu@udel.edu, poulakas@udel.edu)
[2]Department of Mechanical Engineering, National Technical University of Athens, Athens, Greece
(E-mail: egpapado@central.ntua.gr)

Abstract: This paper studies the control of quadrupedal bounding in the presence of torso flexibility and non-trivial leg inertia, and it proposes a method for speed transitioning based on the sequential composition of locally stable bounding gaits corresponding to different running speeds. First, periodic bounding motions are generated simply by positioning the legs during flight via suitable (virtual) holonomic constraints that are imposed on the evolution of the leg angles; at this stage, no control effort is developed on legs that are in contact with ground, resulting in efficient, nearly passive, bounding gaits. The resulting motions are stabilized by a hybrid control law which coordinates the movement of the torso and the legs in continuous time, and updates the leg touchdown angles in an event-based fashion. Finally, through sums-of-squares (SOS) programming, formally verified estimates of the domain of attraction of stable fixed points are used to realize speed transitions by switching among different bounding gaits in a sequential fashion.

Keywords: Quadrupedal bounding, flexible torso, domain of attraction, sums of squares.

1. INTRODUCTION

Recently, quadrupedal running in the presence of torso flexibility has attracted considerable attention in the context of reduced-order models [2,5,6,17,22]; such models are often termed "templates" in the terminology of [7]. The majority of these efforts focus primarily on establishing conditions under which bounding gaits can be realized passively, through the interaction of the torso oscillations with the leg motion [2,6,17]. In the spirit of the Spring Loaded Inverted Pendulum (SLIP) [7], the aforementioned models typically employ legs that are massless prismatic springs, and – echoing the passively stable SLIP – it was found that stable bounding motions can be passively generated [2, 22], as was the case in rigid-torso bounding models [12].

However, these template-like models cannot be directly applied to develop control laws for more realistic robot models with non-trivial leg mass – such as those in [5, 10], for example. This is due to the fact that the non-trivial dynamics associated with leg recirculation significantly affects the motion of the system [16]. Periodic bounding motions in the presence non-massless legs have been generated in [5] through a PID controller that positions the legs during flight. On the other hand, [10] used a combination of swing-leg retraction with stance-leg impedance control to stabilize bounding; albeit powerful, this method relies on sufficiently actuated legs, and the presence of compliant elements in the leg's structure may require non-trivial modifications.

In this paper, we take advantage of our previous results in [1–3] to propose a control law that combines energy efficient motions with stability. In more detail, to generate bounding motions, the controller uses the hip joint torques merely to recirculate the legs during flight;

† Ioannis Poulakakis is the presenter of this paper.

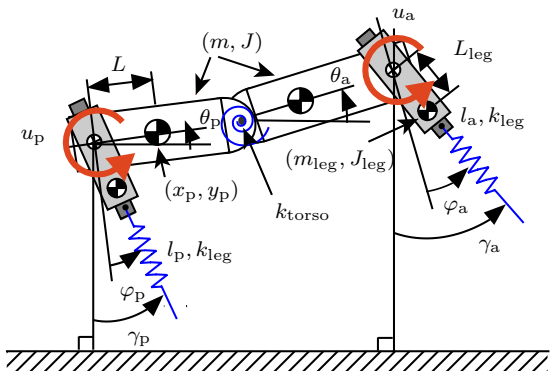

Fig. 1 The sagittal-plane quadrupedal models with torso compliance and leg mass and inertia.

no control effort is developed at the hip of a leg that is in contact with the ground. As a result, the overall motion is generated through the natural interaction between the torso's and the legs' passive springs. To ensure stability of the resulting motions, the controller influences the torso's flexion-extension oscillation using feedback from the angle of the support leg, thereby effectively coordinating the motion of the torso and the legs.

A second aspect investigated in this paper is the regulation of forward velocity. A variety of controllers has been proposed to adjust running speed; these controllers typically modify hip torques during stance or touchdown angles during flight [9, 15, 20]. A different approach has been proposed in [10], where galloping motion over a wide range of running speeds has been generated by "shaping" the vertical ground reaction forces through the hip and knee joint torques of the leg in contact with the ground. However, the requirement of sufficiently actuated legs may restrict this method to models without springy legs.

By way of contrast, in this paper, speed control is formulated as a gait transition problem. A switching

controller is employed to pass from a "source" bounding gait to one with the desired running speed, provided that the fixed point associated with the "source" gait is in the domain of attraction of the fixed point associated with the "target" gait. Estimates of the domain of attraction can be computed based on quadratic Lyapunov functions through sums-of-squares programming as in [19]. It should be mentioned that this method can be used to create more complex gait behaviors by composing different motion primitives in a sequential fashion; see [19] and references therein and our recent work [4] for the implementation on gait transitions.

2. MODEL AND GAIT ASSUMPTIONS

The sagittal-plane quadrupedal model is depicted in Fig. 1. The torso consists of two identical rigid bodies – one represents the posterior and the other the anterior part – connected through a torsional spring to provide compliance. Both the anterior and the posterior legs have the same structure; an upper segment with mass and inertia and and a lower segment represented by a massless spring. The interaction between the toe and the ground is modeled as an unactuated, frictionless pin joint. The physical parameters of the model is shown in Table 1. This model differs from the passive one of [2] in the nonzero leg mass and inertia shown in bold in Table 1.

The bounding gait considered in this work is depicted in Fig. 2. Depending on the state of the legs and the configuration of the torso, the bounding cycle can be divided into four phases: stance-posterior (sp), stance-anterior (sa), flight-gathered (fg) and flight-extended (fe). These phases are separated by touchdown and liftoff events. Note that in the gathered flight, the torso assumes a concave configuration, while in the extended flight it assumes a convex configuration.

3. HYBRID DYNAMICS

With reference to Fig. 1, in the stance phases $i \in \{\mathrm{sp}, \mathrm{sa}\}$, the configuration space Q_i can be parameterized by the length of the leg in contact with the ground – that is, $l_\mathrm{p} \in \mathbb{R}$ for the posterior and $l_\mathrm{a} \in \mathbb{R}$ for the anterior stance phase – the leg angles $(\varphi_\mathrm{p}, \varphi_\mathrm{a}) \in \mathbb{S}^2$ relative to the torso, and the pitch angles of the two segments of the torso – namely, $(\theta_\mathrm{p}, \theta_\mathrm{a}) \in \mathbb{S}^2$, i.e.,

$$q_i := \begin{cases} (l_\mathrm{p}, \varphi_\mathrm{p}, \varphi_\mathrm{a}, \theta_\mathrm{p}, \theta_\mathrm{a})' \in Q_i & \text{for } i = \mathrm{sp}, \\ (l_\mathrm{a}, \varphi_\mathrm{p}, \varphi_\mathrm{a}, \theta_\mathrm{p}, \theta_\mathrm{a})' \in Q_i & \text{for } i = \mathrm{sa}. \end{cases} \quad (1)$$

In the flight phases, the configuration space Q_i, $i \in \{\mathrm{fg}, \mathrm{fe}\}$, can be parameterized by the Cartesian coordinates $(x_\mathrm{p}, y_\mathrm{p}) \in \mathbb{R}^2$ of the COM of the posterior part of the torso, the pitch angles $(\theta_\mathrm{p}, \theta_\mathrm{a}) \in \mathbb{S}^2$ of the posterior and anterior parts of the torso, together with the leg angles $(\varphi_\mathrm{p}, \varphi_\mathrm{a}) \in \mathbb{S}^2$; i.e,

$$q_i := (x_\mathrm{p}, y_\mathrm{p}, \varphi_\mathrm{p}, \varphi_\mathrm{a}, \theta_\mathrm{p}, \theta_\mathrm{a})' \in Q_i \ \text{ for } \ i \in \{\mathrm{fg}, \mathrm{fe}\} \ . \quad (2)$$

The equations that govern the motion of the model in all phases can be derived using the method of Lagrange and are written in state-space form as

$$\begin{aligned} \dot{x}_i &= f_i(x_i) + g_i(x_i) u_i \quad (3) \\ &= f_i(x_i) + g_i^\mathrm{a}(x_i) u_i^\mathrm{a} + g_i^\mathrm{p}(x_i) u_i^\mathrm{p} + g_i^\mathrm{t}(x_i) u_i^\mathrm{t} \end{aligned}$$

where $x_i := (q_i', \ \dot{q}_i')'$ is the state vector for each phase $i \in \{\mathrm{sp}, \mathrm{sa}, \mathrm{fg}, \mathrm{fe}\}$ evolving in $TQ_i := \{(q_i', \ \dot{q}_i')' | \ q_i \in Q_i, \dot{q}_i \in \mathbb{R}^{\dim(Q_i)}\}$. The input $u_i := (u_i^\mathrm{p}, u_i^\mathrm{a}, u_i^\mathrm{t})'$ includes the torques applied at the posterior hip joint, the anterior hip joint and the torso joint, respectively.

The continuous-time phases are separated by discrete events. The flight phases terminate when the vertical distance between the toe of either the posterior or the anterior leg and the ground becomes zero. Due to the non-negligible mass of the upper leg, an impact occurs at touchdown which is modeled as in [1, 3]. On the other hand, transitions from stance to flight occur when the vertical ground reaction force reduces to zero.

Table 1 Mechanical Parameters of the Model

Parameter	Value	Units
Half Torso Mass (m)	10.432	kg
Half Torso Inertia (J)	0.36	kgm^2
Hip-to-COM Spacing (L)	0.138	m
Nominal Leg Length (l_0)	0.36	m
Leg Spring Constant (k_leg)	7329	N/m
Torso Spring Constant (k_torso)	203	Nm/rad
Leg Mass (m_leg)	**1**	kg
Leg Inertia (I_leg)	**0.001**	kgm^2
Hip-to-Leg COM Spacing (L_Leg)	**0.09**	m

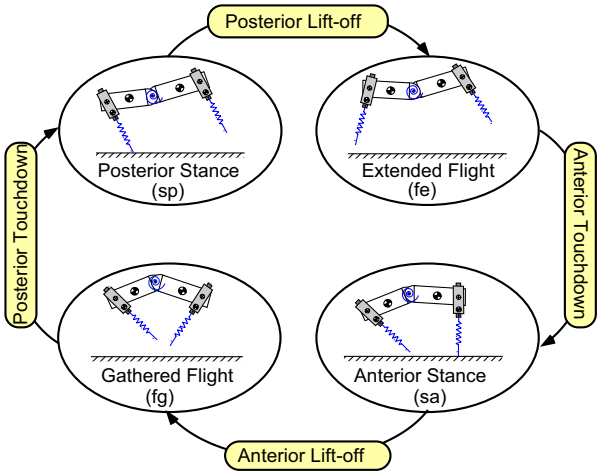

Fig. 2 Bounding phases and events.

4. LEG RECIRCULATION: GENERATING PERIODIC MOTIONS

The objective of this section is to generate periodic bounding motions with the model of Fig. 1. Because of the non-trivial leg mass and inertia, periodic bounding motions cannot be generated passively as in [2]. However, we can still take advantage of the passive dynamics

associated with the torso and leg springs in exciting periodic motions. In more detail, in generating bounding motions, the torso joint will be unactuated throughout the phases, i.e., $u_i^{\mathrm{t}} = 0$ for $i \in \{\mathrm{sp}, \mathrm{sa}, \mathrm{fe}, \mathrm{fg}\}$, while the hip joint is actuated *only* when the corresponding leg is in flight so that the controller merely swings the leg forward to the desired touchdown angle.

The design of the controller begins by associating a output function of the form

$$y_i = q_{\mathrm{c},i} - h_i^{\mathrm{d1}}(s_i(q_i), \alpha_i, \beta_i) \ , \tag{4}$$

to the dynamics (3) where $i \in \{\mathrm{sa}, \mathrm{fg}, \mathrm{sp}, \mathrm{fe}\}$. In (4), $q_{\mathrm{c},i}$ is the controlled variable and h_i^{d1} represents its desired evolution that is parameterized via a set of parameters α_i, β_i as detailed below. The controlled variables are defined by

$$q_{\mathrm{c},i} := \begin{cases} \gamma_{\mathrm{p}} = \varphi_{\mathrm{p}} + \theta_{\mathrm{p}} & \text{for } i = \mathrm{sa}, \\ \gamma_{\mathrm{a}} = \varphi_{\mathrm{a}} + \theta_{\mathrm{a}} & \text{for } i = \mathrm{sp}, \\ (\gamma_{\mathrm{p}}, \gamma_{\mathrm{a}})' & \text{for } i \in \{\mathrm{fe}, \mathrm{fg}\}. \end{cases} \tag{5}$$

In (4), $s_i \in [0, 1]$ is a monotonically increasing quantity defined as

$$s_i := \frac{x_{\mathrm{p},i}^{\max} - x_{\mathrm{p}}}{x_{\mathrm{p},i}^{\max}} \tag{6}$$

where $x_{\mathrm{p},i}^{\max}$ is the travelled distance of the COM of the posterior torso in each phase. Note that y_i is only a function of q_i, and thus can be interpreted as a holonomic constraint to the system.

4.1. Designing the constraints

4.1.1. Posterior Stance

As was mentioned above, during the posterior stance phase, the hip joint of the leg in contact with the ground is unactuated $u_{\mathrm{sp}}^{\mathrm{p}} = 0$, and the only input that acts on the system is applied at the hip of the anterior leg with the objective of placing the anterior leg at a desired touchdown angle. Hence, the dynamics (3) becomes

$$\dot{x}_{\mathrm{sp}} = f_{\mathrm{sp}}(x_{\mathrm{sp}}) + g_{\mathrm{sp}}^{\mathrm{a}}(x_{\mathrm{sp}}) u_{\mathrm{sp}}^{\mathrm{a}} \ . \tag{7}$$

The desired evolution $h_{\mathrm{sp}}^{\mathrm{d1}}$ of the absolute anterior leg angle is parameterized via a 3rd-order Beziér polynomial with coefficients $\alpha_{\mathrm{sp}} := \{\alpha_{\mathrm{sp},k}\}_{k=0,1}$ and $\beta_{\mathrm{sp}} := \{\beta_{\mathrm{sp},k}\}_{k=0,1}$; i.e.,

$$h_{\mathrm{sp}}^{\mathrm{d1}}(s_{\mathrm{sp}}(q_{\mathrm{sp}}), \alpha_{\mathrm{sp}}, \beta_{\mathrm{sp}}) = \sum_{k=0}^{1} b_{\mathrm{sp},k}(s_{\mathrm{sp}}(q_{\mathrm{sp}})) \alpha_{\mathrm{sp},k} + b_{\mathrm{sp},2}(s_{\mathrm{sp}}(q_{\mathrm{sp}})) \beta_{\mathrm{sp},0} + b_{\mathrm{sp},3}(s_{\mathrm{sp}}(q_{\mathrm{sp}})) \beta_{\mathrm{sp},1} \ , \tag{8}$$

where the terms $b_{\mathrm{sp},k}$ are given by

$$b_{\mathrm{sp},k}(s_{\mathrm{sp}}) := \frac{3!}{k!(3-k)!} s_{\mathrm{sp}}^k (1 - s_{\mathrm{sp}})^{3-k} \ .$$

Using properties of Beziér polynomials [21],

$$h_{\mathrm{sp}}^{\mathrm{d1}}(1) = \beta_{\mathrm{sp},1}, \quad \left. \frac{\partial h_{\mathrm{sp}}^{\mathrm{d1}}}{\partial s_{\mathrm{sp}}} \right|_{s_{\mathrm{sp}}=1} = 3(\beta_{\mathrm{sp},1} - \beta_{\mathrm{sp},0}) \ , \tag{9}$$

which implies that selecting $\beta_{\mathrm{sp},0} = \beta_{\mathrm{sp},1}$ results in nominal bounding gaits where the anterior leg touches down at an angle equal to $\beta_{\mathrm{sp},1}$ and with zero angular velocity.

4.1.2. Extended Flight

During the extended flight, the posterior leg swings forward while the anterior leg maintains a constant angle $\beta_{\mathrm{sp},1}$ in anticipation to touchdown. The corresponding hip torques $u_{\mathrm{sa}}^{\mathrm{p}}$ and $u_{\mathrm{sa}}^{\mathrm{a}}$ are both available for control, and the output is defined as

$$h_{\mathrm{fe}}^{\mathrm{d1}}(s_{\mathrm{fe}}(q_{\mathrm{fe}}), \alpha_{\mathrm{fe}}) = \begin{bmatrix} \sum_{k=0}^{3} b_{\mathrm{fe},k}(s_{\mathrm{fe}}(q_{\mathrm{fe}})) \alpha_{\mathrm{fe},k} \\ \beta_{\mathrm{sp},1} \end{bmatrix}. \tag{10}$$

where α_{fe} includes the Beziér polynomial coefficients and b_{fe} is determined similarly to (9).

4.1.3. Anterior Stance

During the anterior stance phase, the leg in contact with the ground is unactuated $u_{\mathrm{sa}}^{\mathrm{a}} = 0$, so that

$$\dot{x}_{\mathrm{sa}} = f_{\mathrm{sa}}(x_{\mathrm{sa}}) + g_{\mathrm{sa}}^{\mathrm{p}}(x_{\mathrm{sa}}) u_{\mathrm{sa}}^{\mathrm{p}} \tag{11}$$

The desired evolution of the posterior leg angle is

$$h_{\mathrm{sa}}^{\mathrm{d1}}(s_{\mathrm{sa}}(q_{\mathrm{sa}}), \alpha_{\mathrm{sa}}, \beta_{\mathrm{sa}}) = \sum_{k=0}^{1} b_{\mathrm{sa},k}(s_{\mathrm{sa}}(q_{\mathrm{sa}})) \alpha_{\mathrm{sa},k} + b_{\mathrm{sa},2}(s_{\mathrm{sa}}(q_{\mathrm{sa}})) \beta_{\mathrm{sa},0} + b_{\mathrm{sa},3}(s_{\mathrm{sa}}(q_{\mathrm{sa}})) \beta_{\mathrm{sa},1} \ . \tag{12}$$

Again, we set $\beta_{\mathrm{sa},0} = \beta_{\mathrm{sa},1}$ so that the posterior leg arrives at the angle $\beta_{\mathrm{sa},1}$ with zero angular velocity at the end of the anterior stance.

4.1.4. Gathered Flight

Similarly to the extended flight phase, in the gathered flight phase, the posterior leg maintains a constant angle while the anterior leg evolves according to the output

$$h_{\mathrm{fg}}^{\mathrm{d1}}(s_{\mathrm{fg}}(q_{\mathrm{fg}}), \alpha_{\mathrm{fg}}) = \begin{bmatrix} \beta_{\mathrm{sa},1} \\ \sum_{k=0}^{3} b_{\mathrm{fg},k}(s_{\mathrm{fg}}(q_{\mathrm{fg}})) \alpha_{\mathrm{fg},k} \end{bmatrix}. \tag{13}$$

4.2. Imposing the constraints

To impose the constraints (4) on the dynamics (3) we differentiate (4) twice with respect to time to obtain

$$\frac{d^2 y_i}{dt^2} = L_{f_i}^2 y_i(x_i, \alpha_i, \beta_i) + L_{g_{i,\mathrm{a}}} L_{f_i} y_i(q_i, \alpha_i, \beta_i) u_{i,\mathrm{a}} + L_{g_{i,\mathrm{p}}} L_{f_i} y_i(q_i, \alpha_i, \beta_i) u_{i,\mathrm{p}} \ , \tag{14}$$

where $L_{f_i}^2 y_i$, $L_{g_{i,\mathrm{a}}} L_{f_i} y_i$ and $L_{g_{i,\mathrm{p}}} L_{f_i} y_i$ are the Lie derivatives of the output function y_i defined by (4) along the vector fields f_i, $g_{i,\mathrm{a}}$ and $g_{i,\mathrm{p}}$ that participate in (3); see [21] for detailed definitions. In each phase, the inputs available – i.e., $(u_{i,\mathrm{p}}, u_{i,\mathrm{a}})$ in the gathered and extended flight phases, $u_{i,\mathrm{p}}$ in the anterior stance and $u_{i,\mathrm{a}}$ in the posterior stance – are selected to ensure $\frac{d^2 y_i}{dt^2} = 0$.

4.3. Poincaré Map

The dynamics of bounding can be described by concatenating the continuous-time phases according to the sequence of Fig. 2. To study the existence of periodic motions, the method of Poincaré is used with the Poincaré section taken right after the anterior leg liftoff, i.e.,

$$\mathcal{S} := \{x_{\mathrm{fg}} \in TQ_{\mathrm{fg}} \mid y_{\mathrm{p}} - y_{\mathrm{p}}^* = 0\} \ , \tag{15}$$

where $y_{\rm p}^* = l_0\cos(\theta_{\rm a}+\varphi_{\rm a}) + 2L\cos\theta_{\rm a} - L\cos\theta_{\rm p}$. By projecting out the monotonically increasing horizontal coordinate $x_{\rm p}$ from the state vector $x_{\rm fg}$ and substituting $y_{\rm p}$ through the condition defining (15), the (reduced) Poincaré map can be defined as

$$z[k+1] = \mathcal{P}_1(z[k], \alpha[k], \beta[k]) \ , \qquad (16)$$

where z represents the remaining states in $x_{\rm fg}$, i.e.,

$$z := [\theta_{\rm p}, \theta_{\rm a}, \varphi_{\rm p}, \varphi_{\rm a}, \dot{x}_{\rm p}, \dot{y}_{\rm p}, \dot{\theta}_{\rm p}, \dot{\theta}_{\rm a}, \dot{\varphi}_{\rm p}, \dot{\varphi}_{\rm a}] \qquad (17)$$

and $\alpha = \{\alpha_i, x_{{\rm p},i}^{\max}, x_{{\rm p},i}^{\min}\}$ for $i \in \{{\rm sp}, {\rm sa}, {\rm fe}, {\rm fg}\}$, $\beta = \{\beta_{\rm sa}, \beta_{\rm sp}\}$ including all the parameters participating in the leg recirculation controller. Then, the problem of computing periodic bounding gaits becomes equivalent to finding a state vector z so that

$$z - \mathcal{P}_1(z, \alpha, \beta) = 0 \qquad (18)$$

for suitable parameter values α and β and is solved numerically using MATLAB's `fmincon`.

Fig. 3 shows the evolution of forward velocity $x_{\rm p}$, torso oscillation $\theta_{\rm a} - \theta_{\rm p}$, absolute leg angles $(\gamma_{\rm p}, \gamma_{\rm a})$ and the hip torque input $(u^{\rm p}, u^{\rm a})$ of a representative fixed point. Note that in Fig. 3(b) there is one torso flexion-extension oscillation in one stride, as in the passively generated bounding motions of [2]. Also, the maximum and minimum torso angle occur in the extended and gathered flight phases, corresponding to the convex and concave configurations, respectively.

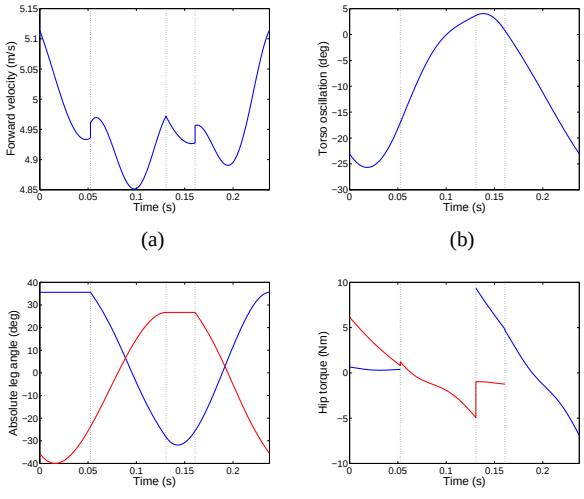

Fig. 3 Evolution of forward velocity (a), torso oscillation (b), absolute leg angles (c) and hip joint torque (d) of a fixed point. In (c) and (d), the red and blue lines correspond to the anterior and posterior legs, respectively. The vertical lines separate one cycle into four phases: from left to right, fg, sp, fe and sa. The discontinuities are due to the impact at touchdown.

4.4. Local Stability

To analyze the local stability properties of bounding, we linearize (16) at a fixed point $\bar{z}$ assuming α and β are constants:

$$\Delta z[k+1] = A_1 \Delta z[k], \qquad (19)$$

where $\Delta z = z - \bar{z}$ and $A_1 = \frac{\partial \mathcal{P}_1}{\partial z}\big|_{z=\bar{z}}$. When the eigenvalues of A_1 are all within the unit disc, the corresponding fixed point is locally exponentially stable. The generated fixed points are not stable, thus a controller is necessary to sustain periodic bound orbits in the presence of perturbations.

5. LEG-TORSO COORDINATION: STABILIZING PERIODIC MOTIONS

In our previous work [2], a hybrid controller has been proposed to stabilize nearly passive bounding motions in a model with massless legs. The controller of [2] introduces an active component $u^{\rm t}$ of the torso joint torque that acts in parallel with the torsional spring connecting the posterior and anterior parts of the torso. Then, $u^{\rm t}$ is used as a control input to influence the coordination between the torso's flexion-extension oscillations and the motion of the legs [2]. In this paper, a similar control approach is adopted in the higher-dimensional setting of the model of Fig. 1 to stabilize the bounding motions generated with the leg recirculation controller of Section 4.

In more detail, in each phase of the bounding cycle, the system (3) in closed loop with the corresponding action of the leg recirculation controller takes the form

$$\dot{x}_i = f_i^{\rm cl}(x_i) + g_i^{\rm t}(x_i) u_i^{\rm t}, \qquad (20)$$

where $u^{\rm t}$ represents the input torque acting in parallel with the torso spring; recall that $u^{\rm t}$ was not used in the controller of Section 4 that generates bounding motions. Here, $u_i^{\rm t}$ is employed in the stance phases to impose holonomic constraints on (20) that coordinate the motion of the torso and legs according to a nominal bounding orbit, as was generated in Section 4. Finally, a discrete-time controller is engaged to ensure local exponential stability of the resulting motions.

5.1. Continuous-time Control

For the stance phases $i \in \{{\rm sp}, {\rm sa}\}$ we associate to the closed-loop dynamics (20) the output function

$$y_i = (\theta_{\rm a} - \theta_{\rm p}) - h_i^{\rm d2}(\varsigma_i(q_i), \eta_i) \qquad (21)$$

where $h_i^{\rm d2}$ is the desired output of the relative pitch angle $\theta_{\rm a} - \theta_{\rm p}$. Through designing $h_i^{\rm d2}$, the information about the leg-torso coordination pattern that characterizes the selected generated gait is passed to the feedback controller. In more detail, $h_i^{\rm d2}$ is designed through a suitable parameterization of the relative pitch angle $(\theta_{\rm a} - \theta_{\rm p})$ at the desired gait generated in Section 4, i.e.,

$$h_i^{\rm d2}(\varsigma_i(q_i)) = \sum_{k=0}^{3} c_{i,k}(\varsigma_i(q_i))\eta_{i,k} \ , \qquad (22)$$

where $\eta_{i,k}$ are the Beziér coefficients, $c_{i,k}$ are given by

$$c_{i,k}(\varsigma_i) := \frac{3!}{k!(3-k)!}\varsigma_i^k(1-\varsigma_i)^{3-k} \ , \qquad (23)$$

and ς_i, $i \in \{{\rm sp}, {\rm sa}\}$, are the strictly monotonic quantities

$$\varsigma_{\rm sa} := \frac{\gamma_{\rm a}^{\max} - \gamma_{\rm a}}{\gamma_{\rm a}^{\max} - \gamma_{\rm a}^{\min}} \quad \text{and} \quad \varsigma_{\rm sp} := \frac{\gamma_{\rm p}^{\max} - \gamma_{\rm p}}{\gamma_{\rm p}^{\max} - \gamma_{\rm p}^{\min}} \ ,$$

in which $\gamma_{\rm a}^{\max}$ and $\gamma_{\rm a}^{\min}$ are the maximum and minimum values of $\gamma_{\rm a}$ and similarly $\gamma_{\rm p}^{\max}$ and $\gamma_{\rm p}^{\min}$ are the corresponding values for $\gamma_{\rm p}$. In words, the evolution of the relative pitch angle during the stance phases is determined by the absolute leg angle of the unactuated leg in contact with the ground.

Finally, as in [21], the constraints (22) are imposed on the system (20) in an asymptotic fashion, i.e.,

$$u_i^{\rm t} = (L_{g_i^{\rm t}} L_{f_i^{\rm cl}} y_i)^{-1} [\nu(y_i, \dot{y}_i, \epsilon) - L_{f_i^{\rm cl}}^2 y_i(x_i)] \quad (24)$$

where $\nu = -\frac{1}{\epsilon^2} K_{\rm P} y_i - \frac{1}{\epsilon} K_{\rm V} \dot{y}_i$. $K_{\rm P}, K_{\rm V}$ are positive gains and $\epsilon > 0$.

5.2. Discrete-time Control

By the construction of our feedback law, the parameter array β includes the absolute leg angles at touchdown, which (partially) determine when the corresponding gathered and extended flight phases are terminated. A variety of control procedures is available for updating these angles in an event-based fashion to enhance stability; see [15] or [18] for examples. In this work, a discrete Linear Quadratic Regulator (LQR) is employed that positions the legs during flight based on feedback of the states at the Poincaré section, similarly to [13]. In more detail, denoting $\eta = \{\eta_{\rm sa}, \eta_{\rm sp}, \gamma_{\rm p}^{\max}, \gamma_{\rm a}^{\max}, \gamma_{\rm p}^{\min}, \gamma_{\rm a}^{\min}\}$, the Poincaré return map in closed loop with the continuous-time controller of Section 5.1 becomes

$$z[k+1] = \mathcal{P}_1(z[k], \alpha[k], \beta[k], \eta[k]) \ .$$

In what follows, the parameters α and η are kept constant and equal to their nominal values, while the touchdown angles $\beta[k]$ will be updated in a step-by-step fashion. To emphasize the fact that $\beta[k]$ includes inputs availabe for control in discrete time, we define

$$z[k+1] = \mathcal{P}_2(z[k], \beta[k]) \ . \quad (25)$$

Linearizing (25) at a fixed point $\bar{z}$ results in

$$\Delta z[k+1] = A_2 \Delta z[k] + B_2 \Delta\beta[k] \quad (26)$$

where $\Delta z = z - \bar{z}$, $\Delta\beta = \beta - \bar{\beta}$, $A_2 = \frac{\partial \mathcal{P}_2}{\partial z}|_{z=\bar{z},\beta=\bar{\beta}}$ and $B_2 = \frac{\partial \mathcal{P}_2}{\partial \beta}|_{z=\bar{z},\beta=\bar{\beta}}$. Define the cost function

$$J(\Delta z) = \sum_{i=k}^{\infty} (\Delta z' Q \Delta z + \Delta\beta' R \Delta\beta), \quad (27)$$

where $Q = Q' \geq 0, R = R' > 0$. It can be shown that the optimal cost-to-go J^* is given by

$$J^*(\Delta z) = \Delta z' S \Delta z, \quad S' = S > 0 \quad (28)$$

where S is the solution of the associated discrete-time Riccati equation. The optimal feedback policy updates the swing-leg retraction angles according to

$$\Delta\beta[k] = -K \Delta z[k] \ . \quad (29)$$

where K is derived from S as

$$K = (B_2' S B_2 + R)^{-1} (B_2' S A_2) \ ,$$

and K and S are given by MATLAB's `dlqr`. With the controller (29), the closed-loop return map becomes

$$z[k+1] = \mathcal{P}_2(z[k], \bar{\beta} - K\Delta z[k]) := \mathcal{P}_3(z[k]) \ , \quad (30)$$

and all the eigenvalues of the Jacobian $\frac{\partial \mathcal{P}_3}{\partial z}$ are located within the unit disc. To illustrate the orbit's local stability, the state prior to liftoff of the bounding motion in Fig. 3 is perturbed away from the fixed point by an initial error of $+0.1{\rm m/s}$ in $\dot{x}_{\rm p}$ and $-3{\rm deg}$ in $\theta_{\rm a}$. The system converges back to the nominal motion as shown in Fig. 4. Note that the toe/ground interaction constraints are respected and the maximum torso torque is less than $40{\rm Nm}$.

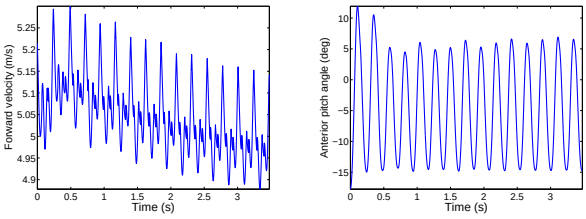

(a) (b)

Fig. 4 The evolution of the forward velocity and the anterior pitch angle when the system is perturbed with $+0.1{\rm m/s}$ in $\dot{x}_{\rm p}$ and $-3{\rm deg}$ in $\theta_{\rm a}$.

6. SPEED TRANSITIONS

As was mentioned in the introduction, in this work, speed transitions will be realized by switching between limit cycles according to the schematic of Fig. 5. In Fig. 5, the limit cycles ϕ_0 and ϕ_1 represent periodic bounding motions at different running speeds, the surfaces $\mathcal{S}_0$ and $\mathcal{S}_1$ denote suitable Poincaré sections and $\bar{z}_0$ and $\bar{z}_1$ are the corresponding fixed points. The domain of attraction of each of the fixed points $\bar{z}_0$ and $\bar{z}_1$ on $\mathcal{S}_0$ and $\mathcal{S}_1$ is denoted[1] by $\mathcal{D}_0$ and $\mathcal{D}_1$, respectively. By examining the relationship between the domains of attraction and the fixed points, the feasibility of generating a transition can be determined. For example, as shown in Fig. 5, if $\bar{z}_0 \in \mathcal{D}_1$, then employing a switching controller $\Gamma_{0\to1}$,

$$\Gamma_{0\to1} : \{(\alpha_0, \beta_0, \eta_0, K_0) \to (\alpha_1, \beta_1, \eta_1, K_1)\} \ , \quad (31)$$

which effectively changes the controller parameters from those corresponding to the orbit ϕ_0 to those of ϕ_1, the motion of the system will be attracted by the target orbit ϕ_1. Symbolically, if $\bar{z}_0 \in \mathcal{D}_1$, then $\bar{z}_0 \xrightarrow{\Gamma_{0\to1}} \bar{z}_1$. Furthermore, if $\bar{z}_1 \in \mathcal{D}_0$, then two-way transitions can be realized enabling both acceleration and deceleration; such transitions will be denoted as $\bar{z}_0 \underset{\Gamma_{1\to0}}{\overset{\Gamma_{0\to1}}{\leftrightarrows}} \bar{z}_1$.

Generally, determining the domain of attraction is a difficult task, even for low dimensional systems. However, for the system (30), the state space of which is ten dimensional, we will provide suitable *estimates* of the domain of attraction of a bounding fixed point, using quadratic Lyapunov functions [8], and sums of squares verification [11, 19], as detailed in the following section.

[1] Note that $\mathcal{D}_0$ and $\mathcal{D}_1$ do not represent the domains of attraction of the entire periodic orbits ϕ_0 and ϕ_1.

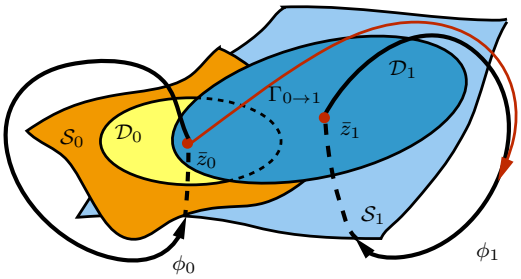

Fig. 5 A conceptual illustration of the transition between two different limit cycles, i.e., ϕ_0 and ϕ_1. $\mathcal{S}_0$ and $\mathcal{S}_1$ are the Poincaré sections of ϕ_0 and ϕ_1, and $\bar{z}_0$ and $\bar{z}_1$ are the corresponding fixed points. $\mathcal{D}_0$ and $\mathcal{D}_1$ are the domain of attractions at the Poincaré sections for ϕ_0 and ϕ_1, respectively.

6.1. Estimation of Domain of Attraction

For ease of implementation, the fixed point is translated to the origin. Since $\Delta z[k] = z[k] - \bar{z}$, (30) implies

$$\Delta z[k+1] = \mathcal{P}_3(\bar{z} + \Delta z[k]) - \bar{z} \ , \tag{32}$$

which represents a map from $\Delta z[k]$ to $\Delta z[k+1]$; i.e.,

$$\Delta z[k+1] = \mathcal{P}_4(\Delta z[k]) \ . \tag{33}$$

The fixed point corresponding to (33) is $\Delta z[k] = 0$ and its domain of attraction can be used to determine the domain of attraction of (30) in a straightforward manner.

A function $V(\Delta z)$ is a valid Lyapunov function for the system (33) if $V(\Delta z)$ is positive definite and $V(\Delta z)[k+1] - V(\Delta z)[k] < 0$ in a bounded domain $\mathcal{D}$; we consider domains of the form

$$\mathcal{D}(\rho) := \{\Delta z \mid 0 \le V(\Delta z) \le \rho\} \ , \tag{34}$$

where ρ is a positive scalar. Note that the linear optimal cost-to-go function (28) is already a Lyapunov function candidate since S is a positive definite matrix. Thus, defining $V(\Delta z) := J^*(\Delta z)$, the problem of estimating the domain of attraction takes the form

$$\begin{aligned} &\max \rho \\ &\text{s.t } \forall \Delta z \in \mathcal{D}(\rho), J^*_+(\Delta z[k]) < 0 \end{aligned} \tag{35}$$

where $J^*_+(\Delta z[k]) = J^*(\Delta z[k+1]) - J^*(\Delta z[k])$.

One way to check that the Lyapunov function is decreasing within the domain $\mathcal{D}$ is to formulate a sums-of-squares (SOS) feasibility problem [11] as shown in [19]. A multivariate polynomial $h(x) := h(q_1, ..., q_n)$ is a sum of squares if there exist polynomials $f_1(x), ..., f_m(x)$ such that

$$h(x) = \sum_{i=1}^{m} f_i^2(x), \tag{36}$$

Condition (36) is equivalent to the existence of a positive semidefinite matrix H such that

$$h(x) = Z'(x) H Z(x), \tag{37}$$

where $Z(x)$ is a suitably chosen vector of monomials. For a given polynomial, sums-of-squares programming will check the non-negativity of the polynomial h by searching for a positive semidefinite matrix H [11] .

With the SOS technique, the problem in (35) can be formulated as:

$$\begin{aligned} &\max \rho \\ &\text{s.t } h(\Delta z) \text{ is SOS} \\ &-J^*_+(\Delta z[k]) - h(\Delta z[k])(\rho - J^*(\Delta z[k])) \text{ is SOS,} \end{aligned} \tag{38}$$

where $h(\Delta z)$ is a positive definite polynomial of Δz. Note that the SOS algorithm requires $J^*_+(\Delta z[k])$ to be a polynomial [14]. However, in our case,

$$\begin{aligned} J^*_+(\Delta z[k]) &= \Delta z'[k+1] S \Delta z[k+1] - \Delta z'[k] S \Delta z[k] \\ &= \mathcal{P}_4(z[k])' S \mathcal{P}_4(z[k]) - \Delta z'[k] S \Delta z[k] \ , \end{aligned} \tag{39}$$

in which $\mathcal{P}_4(z[k])$ is not available in closed form; it is obtained through numerical integration. Hence, to proceed with the method, we approximate the return map (33) by expanding $\mathcal{P}_4$ in Taylor series keeping terms up to second order; i.e.,

$$\mathcal{P}_4(\Delta z[k]) \approx T_1 \Delta z[k] + \Delta z'[k] T_2 \Delta z[k] \ , \tag{40}$$

where $T_1 = \frac{\partial \mathcal{P}_4}{\partial \Delta z_i}|_{\Delta z=0}$ and $T_2 = \frac{1}{2}\frac{\partial^2 \mathcal{P}_4}{\partial \Delta z_i \partial \Delta z_j}|_{\Delta z=0}$ for $i, j \in \{1, 2, ..., 10\}$. Substituting (40) into (39) yields

$$\begin{aligned} J^*_+(\Delta z[k]) = (T_1 \Delta z[k] + \Delta z'[k] T_2 \Delta z[k])' \, S \, (T_1 \Delta z[k] \\ + \Delta z'[k] T_2 \Delta z[k]) - \Delta z'[k] S \Delta z[k] \ . \end{aligned} \tag{41}$$

Given the polynomial expression (41), the SOS feasibility program in (38) can be solved by any available SOS toolbox, such as SOSTOOLS [14], and the maximum value $\rho^{\max}$ can be determined by a binary search for the value of ρ above which the SOS feasibility problem fails.

Given $\rho^{\max}$, the largest magnitude of tolerable single perturbation can be calculated for all the states as

$$\Delta z^{\max}(i) = \sqrt{\frac{\rho^{\max}}{S(i,i)}} \tag{42}$$

for $i = 1, 2, ...10$, which provides an indication of the capability of the system in dealing with perturbations. For the fixed point in Fig. 4, $\Delta z^{\max} = (0.03, 0.03, 0.30, 0.04, 0.15, 0.13, 0.31, 0.37, 0.91, 0.90)$.

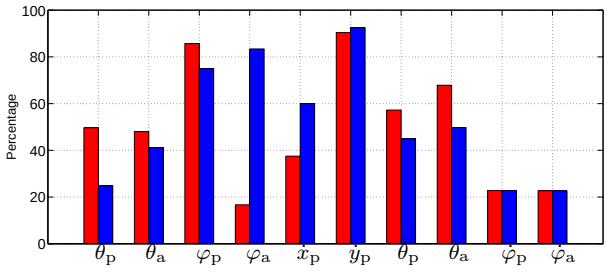

Fig. 6 Ratio of the largest single perturbation that can be tolerated as is predicted by the SOS method over the corresponding value obtained by numerical simulation. The red and blue bars correspond to the positive and negative perturbations, respectively.

Fig. 6 shows the ratio of these values to the values obtained from simulation for the representative fixed point. In the simulation method, a disturbance is regarded as tolerable if the error in the sates is less that 5% after 15 strides. It can be seen from Fig. 6 that the ratio is very diverse among different states. For instance, in the positive direction of $\varphi_{\rm a}$, the SOS method can only capture less than 20% of the nominal value that can be accommodated. On the other hand, in the negative direction of $\dot{y}_{\rm p}$, more than 90% can be described by $\Delta z^{\max}$, implying that $\rho^{\max}$ is constrained by the capability of the system in dealing with negative disturbance in $\dot{y}_{\rm p}$. This observation is consistent with our previous studies in [2], implying that perturbations that tend to decrease hopping height may result in toe stubbing and failure to run due to the lack of active control over leg length.

6.2. A Construction for Speed Transition

In this section, we illustrate the procedure in the context of transitioning between fixed points at different running speeds. As shown in Fig. 7, the fixed point $\bar{z}_0$ is computed and its domain of attraction $\mathcal{D}_0$ is estimated. Because the estimate of the domain of attraction lies in a high dimensional state space, Fig. 7 only shows its projection on the $(\dot{x}_{\rm p}, \dot{y}_{\rm p})$ plane. The fixed points $\bar{z}_1$ and $\bar{z}_2$ are both located within $\mathcal{D}_0$, and have been computed by adding an inequality constraint when searching for them that characterizes their "distance" from $\bar{z}_0$; namely,

$$(\bar{z}_i - \bar{z}_0)' S_0 (\bar{z}_i - \bar{z}_0) \leq \rho_0^{\max} \tag{43}$$

for $i \in \{1, 2\}$. The forward running speed of $\bar{z}_1$ and $\bar{z}_2$ is $5.9{\rm m/s}$ and $5.5{\rm m/s}$, respectively. After estimating the domains of attraction $\mathcal{D}_1$ of $\bar{z}_1$ and $\mathcal{D}_2$ of $\bar{z}_2$, transitions between the fixed points can be easily realized. First, since $\bar{z}_1, \bar{z}_2 \in \mathcal{D}_0$, then the transitions $\bar{z}_1 \xrightarrow{\Gamma_{1\to 0}} \bar{z}_0$ and $\bar{z}_2 \xrightarrow{\Gamma_{2\to 0}} \bar{z}_0$ are both feasible; these transitions are represented by the blue solid lines in Fig. 7. Reversely, $\bar{z}_0 \xrightarrow{\Gamma_{0\to 1}} \bar{z}_1$ can be realized, as the green solid line in Fig. 7 shows, while $\bar{z}_0 \xrightarrow{\Gamma_{0\to 2}} \bar{z}_2$ is not possible since $\bar{z}_0 \notin \mathcal{D}_1$. To realize the transition from $\bar{z}_0$ to $\bar{z}_2$, an intermediate fixed point can be computed that is closer to $\bar{z}_0$ so that its domain of attraction includes $\bar{z}_0$.

By concatenating the basic transitions described above, multi-hop transitions can be realized between fixed points that are further apart. For example, a transition from $\bar{z}_2$ to $\bar{z}_1$ can be achieved using $\bar{z}_0$ as a "bridge" (that is, $\bar{z}_2 \xrightarrow{\Gamma_{2\to 0}} \bar{z}_0 \xrightarrow{\Gamma_{0\to 1}} \bar{z}_1$) corresponding to an increase in the running speed from $5.5{\rm m/s}$ to $5.9{\rm m/s}$. It should be mentioned that the duration of a transition can be decreased by tracking the "distance" to the "target" fixed point. For example, in switching from $\bar{z}_2$ to $\bar{z}_1$, if the states enter the domain of attraction of $\bar{z}_1$ before converging to $\bar{z}_0$, then the switching controller will adopt the controller information of $\bar{z}_1$ in advance, and the evolution of the states will follow the dotted red line without spending time to first converge to $\bar{z}_0$. As shown in Fig. 8, this shortcut decreases the transition time by 28% from $7.2{\rm s}$ to $5.2{\rm s}$. Finally, we remark that, similar to the expansion of LQR-trees [19], the above procedure can be conducted iteratively such that more fixed points can be connected via their domain of attraction to cover a much larger range of running speeds.

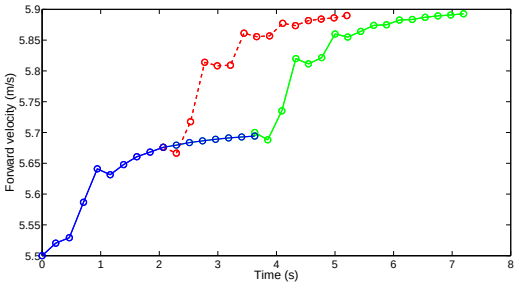

Fig. 8 Two routes of transition from $\bar{z}_2$ to $\bar{z}_1$ in Fig. 7. The red dotted line represents the short-cut.

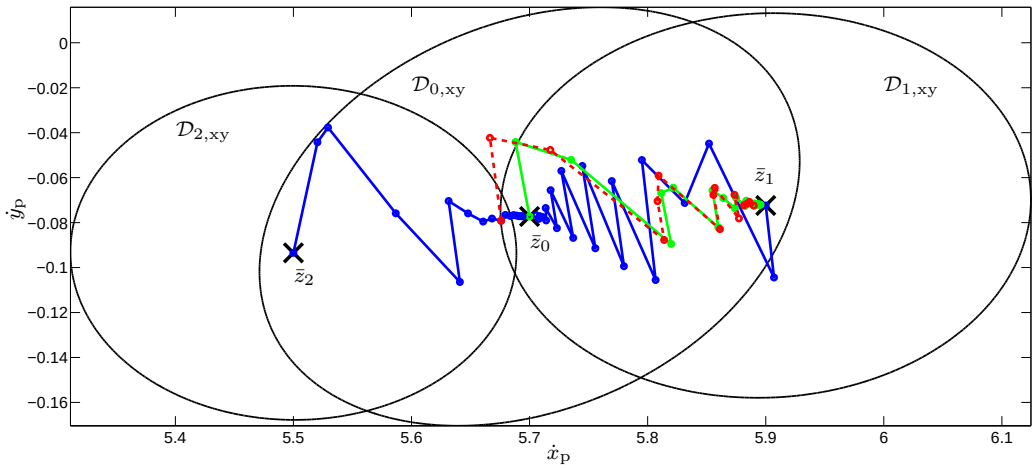

Fig. 7 Transition between fixed points $\bar{z}_0$, $\bar{z}_1$ and $\bar{z}_2$ of different running speeds. $\mathcal{D}_{0,\rm xy}$, $\mathcal{D}_{1,\rm xy}$ and $\mathcal{D}_{2,\rm xy}$ are the projection of their estimated domain of attraction on the $(\dot{x}_{\rm p}, \dot{y}_{\rm p})$ planes when they are only perturbed in this plane. The blue line represents the transition from $\bar{z}_1$, $\bar{z}_2$ to $\bar{z}_0$ while the green line represents the transitions from $\bar{z}_0$ to $\bar{z}_1$. The dotted red line represents a "shortcut" in transition from $\bar{z}_2$ to $\bar{z}_1$.

7. CONCLUSION

This paper proposes a hybrid control law for stabilizing periodic bounding gaits in a sagittal-plane model that features a flexible torso and non-trivial leg mass and inertia. Periodic motions are generated in a nearly passive fashion, merely by recirculating the legs during flight. Local stability is achieved by coordinating the torso oscillation with the leg movement and updating the touchdown angles in a step-by-step fashion. The resulting stable bounding motions are then used to transition between speeds by switching between the corresponding fixed points based on estimates of their domains of attraction verified through sums-of-squares programming.

ACKNOWLEDGMENTS

The work is supported by NSF grant IIS-135072, ARL contract W911NF-12-1-0117, and by the European Union (European Social Fund – ESF) and Greek funds through the Operational Program "Education and Lifelong Learning" of the National Strategic Reference Framework (NSRF) – Research Program: ARISTEIA: Reinforcement of the interdisciplinary and/or inter-institutional research and innovation.

REFERENCES

[1] Q. Cao and I. Poulakakis, "On the energetics of quadrupedal bounding with and without torso compliance," in *Proceedings of the IEEE/RSJ International Conference on Intelligent Robots and Systems*, 2014, pp. 4901–4906.

[2] ——, "Quadrupedal bounding with a segmented flexible torso: passive stability and feedback control," *Bioinspiration & Biomimetics*, vol. 8, no. 4, p. 046007, 2013.

[3] ——, "On the energetics of quadrupedal running: predicting the metabolic cost of transport via a flexible-torso model," *Bioinspiration & Biomimetics*, vol. 10, no. 5, p. 056008, 2015.

[4] Q. Cao, A. van Rijn, and I. Poulakakis, "On the control of gait transitions in quadrupedal running," in *Proceedings of the IEEE/RSJ International Conference on Intelligent Robots and Systems*, Sept. 2015, to appear.

[5] U. Culha and U. Saranli, "Quadrupedal bounding with an actuated spinal joint," in *Proceedings of the IEEE International Conference on Robotics and Automation*, 2011, pp. 1392–1397.

[6] Q. Deng, S. Wang, W. Xu, J. Mo, and Q. Liang, "Quasi passive bounding of a quadruped model with articulated spine," *Mechanism and Machine Theory*, vol. 52, pp. 232–242, 2012.

[7] R. Full and D. E. Koditschek, "Templates and anchors: Neuromechanical hypotheses of legged locomotion on land," *Journal of Experimental Biology*, vol. 202, pp. 3325–3332, 1999.

[8] H. K. Khalil, *Nonlinear Systems*, 3rd ed. Upper Saddle River, NJ: Prentice Hall, 2002.

[9] D. Papadopoulos and M. Buehler, "Stable Running in a Quadruped Robot with Compliant Legs," in *Proceedings of the IEEE International Conference on Robotics and Automation*, 2000, pp. 444–449.

[10] H.-W. Park and S. Kim, "Quadrupedal galloping control for a wide range of speed via vertical impulse scaling," *Bioinspiration & biomimetics*, vol. 10, no. 2, p. 025003, 2015.

[11] P. A. Parrilo, "Structured semidefinite programs and semialgebraic geometry methods in robustness and optimization," Ph.D. dissertation, California Institute of Technology, 2000.

[12] I. Poulakakis, E. G. Papadopoulos, and M. Buehler, "On the stability of the passive dynamics of quadrupedal running with a bounding gait," *The International Journal of Robotics Research*, vol. 25, no. 7, pp. 669–687, 2006.

[13] I. Poulakakis and J. W. Grizzle, "Modeling and control of the monopedal robot Thumper," in *Proc. IEEE Int. Conf. Robotics and Automation ICRA '09*, 2009, pp. 3327–3334.

[14] S. Prajna, A. Papachristodoulou, and P. A. Parrilo, "Sostools: sum of squares optimization toolbox for matlab–users guide," *Control and Dynamical Systems, California Institute of Technology, Pasadena, CA*, vol. 91125, 2004.

[15] M. H. Raibert, *Legged Robots that Balance*. Cambridge, MA: MIT Press, 1986.

[16] J. P. Schmiedeler, R. Siston, and K. J. Waldron, "The significance of leg mass in modeling quadrupedal running gaits," in *ROMANSY 14: Theory and Practice of Robots and Manipulators*, G. Bianchi, J. C. Guinot, and C. Rzymkowski, Eds. Vienna: Springer, 2002, pp. 481–488.

[17] J. E. Seipel, "Analytic-holistic two-segment model of quadruped back-bending in the sagittal plane," in *Proceedings of ASME Mechanisms and Robotics Conference*, vol. 6, 2011, pp. 855–861.

[18] A. Seyfarth, H. Geyer, and H. Herr, "Swing leg retraction: A simple control model for stable running," *Journal of Experimental Biology*, vol. 206, pp. 2547–2555, 2003.

[19] R. Tedrake, I. R. Manchester, M. Tobenkin, and J. W. Roberts, "Lqr-trees: Feedback motion planning via sums-of-squares verification," *The International Journal of Robotics Research*, vol. 29, no. 8, pp. 1038–1052, 2010.

[20] X. Wang, M. Li, P. Wang, and L. Sun, "Running and turning control of a quadruped robot with compliant legs in bounding gait," in *Proceedings of the IEEE International Conference on Robotics and Automation*. IEEE, 2011, pp. 511–518.

[21] E. R. Westervelt, J. W. Grizzle, C. Chevallereau, J. H. Choi, and B. Morris, *Feedback Control of Dynamic Bipedal Robot Locomotion*. Taylor & Francis/CRC Press, 2007.

[22] R. Yamasaki, Y. Ambe, S. Aoi, and F. Matsuno, "Quadrupedal bounding with spring-damper body joint," in *Proceedings of IEEE/RSJ International Conference on Intelligent Robots and Systems*, 2013, pp. 2345–2350.